# Low Temperature Chemical Synthesis of Intermetallic TiFe Nanoparticles for Hydrogen Absorption

**Yasukazu Kobayashi** ( yasu-kobayashi@aist.go.jp )
National Institute of Advanced Industrial Science and Technology
**Shohei Yamaoka**
Waseda University
**Shunta Yamaguchi**
Waseda University
**Nobuko Hanada**
Waseda University
**Shohei Tada**
Ibaraki University
**Ryuji Kikuchi**
University of Tokyo

**Research Article**

**Keywords:** TiFe, CaH2, Chemical, Hydrogen

**Posted Date:** December 10th, 2020

**DOI:** https://doi.org/10.21203/rs.3.rs-121222/v1

# Abstract

Nanosizing of TiFe hydrogen storage alloy is conducted to facilitate its activation. Here, pure intermetallic TiFe nanoparticles (45 nm) were prepared using chemical reduction of oxide precursors at 600 °C, which is the lowest temperature ever used in chemical synthesis. This was achieved using a strong reducing agent ($CaH_2$) in a molten LiCl. When used for hydrogen absorption, the obtained nanoparticles surprisingly exhibited almost no hydrogen absorption. The results demonstrated that TiFe nanoparticles are more difficult to activate than the bulk powder because the oxidized surface layers of the nanoparticles become stabilized, which prevents the morphological change necessary for their activation.


# Introduction

Intermetallic TiFe is an attractive hydrogen-storage material because of its low cost, non-toxicity, and highly reversible hydrogen absorbing/desorbing capacity (~ 1.9 wt%)[1,2]. Reilly and Wiswall reported an excellent hydrogen storage performance of intermetallic hydride forms of TiFeH and $TiFeH_2$[3]. However, the difficulty of TiFe activation is restricting its large-scale application. The treatment is typically conducted under harsh conditions (~ 400 °C and hydrogen pressure ~ 65 atm) because of the passive Ti oxide layer formed on the surface[4]. To improve the TiFe activation kinetics, several approaches, e.g., partial substitution of Ti and Fe by an effective third element and nanostructuring of TiFe powder, were reported. In nanosizing, the hydrogen diffusion into TiFe particles is facilitated by decreasing their size, which allows easy activation under mild conditions[5–8]. Owing to their high scalability and ease of operation, physical methods, such as mechanical alloying and ball milling, are the most common methods to synthesize nanocrystalline TiFe using Ti and Fe pure metals as starting materials[9,10]. Some researchers have investigated using chemical approaches to prepare TiFe nanoparticles from metal salt precursors[11–14]. An electrochemical synthesis, which is conducted under relatively mild conditions, was investigated. This method allows the direct preparation of nanostructured TiFe from oxide precursors, such as titanium ore (ilmenite), $TiO_2$, and $Fe_2O_3$, by passing an electrical current in molten salts. Hua et al. conducted the synthesis at 700 °C by using mixed molten salts ($CaCl_2$–NaCl) instead of pure $CaCl_2$[15–18], which successfully generated fine and homogeneous microstructures of pure TiFe with a particle size of 2–8 μm. However, at 600 °C, the titanium oxide reduction was incomplete, causing impurities, such as $Fe_2Ti$ and $CaTiO_3$, to form. Thus, chemical synthesis of TiFe nanoparticles under mild conditions is still a highly challenging subject.

Here, intermetallic TiFe nanoparticles were prepared by a chemical method using inexpensive $Fe(NO_3)_2$ and $TiO_2$ as precursors in molten LiCl–$CaH_2$ mixture. The proposed method does not require electricity. The reduction was achieved at 600 °C, which is lower than all temperatures used in previous chemical methods, allowing for a simple experimental setup. This peocess was achieved using calcium hydride as a reducing agent in molten LiCl, where highly oxygen-/vapor-free conditions were maintained. These

conditions promoted the reduction of hard-reducible oxides[19–24]. The hydrogen absorption performance of the prepared TiFe nanoparticles was then evaluated.

## Experimental

# Preparation of the intermetallic TiFe nanoparticles

The intermetallic TiFe nanoparticles were chemically prepared by direct reduction of Ti and Fe oxide precursors. The reduction was conducted in a molten LiCl using $H_2$ flow with $CaH_2$ as the reducing agent[19–24]. First, $Fe(NO_3)_2.6H_2O$ was dissolved in distilled water. The solution was then mixed, and $TiO_2$ nanoparticles (Degussa P25 obtained from the Catalysis Society of Japan as JRC-TIO-4(2)) were suspended in the solution at a molar ratio of Fe/Ti = 1/1. The suspension was stirred and heated overnight at 110 °C until dry. The dried powder was then calcined at 500 °C for 2 h under air atmosphere to obtain Fe oxide-covered $TiO_2$ precursor denoted TiFe(Pre). Next, the precursor was mixed with $CaH_2$ and LiCl in a mortar in a weight ratio of precursor/$CaH_2$/LiCl = 0.2/0.8/0.4. The mixed powder was then loaded in a stainless steel reactor connected to an $H_2$ gas flow system and heated at 600 °C for 2 h under the gas flow. Finally, the treated precursor was crushed in a mortar and rinsed with $NH_4Cl$ aqueous solution (0.1 M) and then distilled water to obtain the final product denoted TiFe(Nano), which was a relatively shiny fine black powder (**Figure S1**). For comparison, TiFe bulk powder, i.e., TiFe(Bulk), was synthesized by conventional arc melting of pure Ti and Fe (NEV-AD 03, Nisshin Giken Co.) under an argon atmosphere. The obtained ingot was crushed and sieved to obtain a powder with a diameter of 300 μm to 2 mm in air before the characterization and measurements of hydrogen absorption and desorption. **Figures S2–S4** show that the bulk powder exhibited a good crystal structure of intermetallic TiFe phase and a homogeneous morphology with a stoichiometric molar ratio of Ti/Fe. It had a relatively large oxygen content, suggesting that the surface consisted of an oxide.

# Hydrogen Absorption Experiments

The hydrogen absorption and desorption properties of TiFe(Bulk) and TiFe(Nano) were measured using a Sieverts-type apparatus constructed by our group. Each sample (200–250 mg) was loaded into a stainless-steel vessel. In the activation process, the sample was heated to 400 °C under vacuum by a rotary pump for 30–60 min. Next, hydrogen was introduced at 0.7 MPa and maintained for 30 min and then vacuumed again for 30 min. After cooling the sample to room temperature, hydrogen was introduced again at 6.5 MPa and maintained for 90–120 min. The activation process was repeated for 3 cycles. After the activation, the hydrogen desorption and absorption were repeated at 30 °C. The initial hydrogen pressure during desorption from TiFe(Bulk) and TiFe(Nano) was 0.14 and 0.26 MPa, respectively, and that of hydrogen absorption was 1.70 MPa for both samples. In the 3-cycle activation series and the following 5-cycle one, hydrogen desorption and absorption were repeated 3 times. In the first activation series of TiFe(Bulk), hydrogen desorption and absorption were repeated for only 2 cycles.

# Characterization

The crystal structure was examined by XRD (SmartLab (3 kW), Rigaku) with CuKα radiation at 40 kV and 45 mA and XRD (Ultima III, Rigaku) with CuKα radiation at 40 kV and 40 mA. The porosity was investigated using $N_2$ adsorption/desorption at − 196 °C (BELLSORP mini-II, Microtrac-BEL). The sample was pretreated at 200 °C for 30 min under vacuum before the measurement. The pore size distribution was analyzed from the measured isotherms using the BJH method. The morphology was observed by SEM (JSM-7800F, JEOL Ltd.) with EDS for elemental analysis of TiFe(Nano). Some samples were observed by SEM device (Hitachi high-technologies S-4800) equipped with an energy dispersive X-ray spectroscopy (EDS, AMETEK, Genesis-APEX2) for elemental analysis. The electronic states of Ti and Fe species were examined by XPS (JEOL JPS-9010TR operating with MgKα radiation). The C 1 s peak (284.6 eV) was used to correct the binding energies. An $Ar^+$ etching ion gun (JEOL XP-HSIG, 600 V, 12 mA, 60 s) was used to remove the surface oxide layer of the sample.

# Results And Discussion

Figure 1a shows a synthesis process of TiFe nanoparticles. The X-ray diffraction (XRD) spectroscopy peaks observed for commercial $TiO_2$ (P25) nanoparticles (the Ti source) were assigned to major anatase $TiO_2$ and minor rutile $TiO_2$ (**Figure S5a**). The crystallite sizes calculated from the Scherrer equation were 22.2 and 36.0 nm, respectively (Table 1). The peaks of TiFe(Pre) powder were attributed to $Fe_9TiO_{15}$, and no peaks of $TiO_2$ or any other Fe oxide were observed (**Figure S5b**). $Fe(NO_3)_2$ mainly reacted with the $TiO_2$ surface at 500 °C to form $Fe_9TiO_{15}$ in the calcination process, and the core–shell-structured oxide precursor nanoparticles were formed (unreacted $TiO_2$ and reacted $Fe_9TiO_{15}$ were the core and shell, respectively, Fig. 1a). Next, the precursor was reduced using $CaH_2$ at 600 °C in molten LiCl. The final product was obtained after rigorous rinsing by $NH_4Cl$ solution. No oxide peaks were observed in the XRD spectra of the final product. The XRD peaks of TiFe(Nano) mostly corresponded to intermetallic TiFe (Fig. 1b). The peaks assigned to $TiFe_{39}$ or/and $TiFe_2$ were also observed around 45° but with negligible intensities compared to those of TiFe. Thus, the oxide precursors of $TiO_2$ and $Fe_9TiO_{15}$ were reduced mainly to intermetallic TiFe in molten LiCl–$CaH_2$ at 600 °C. The crystallite size of the TiFe was calculated to be 46.2 nm, which is much larger than those of the oxides in the precursor. Therefore, the reduced metals could be sintered to grow into large intermetallic nanoparticles. **Figures S6** and **S7** show $N_2$ absorption/desorption isotherms and the corresponding pore size distributions of TiFe(Pre) and TiFe(Nano), respectively. The Brunauer-Emmett-Teller (BET) surface areas are summarized in Table 1. Negligible hysteresis of the isotherms and very small pore volume were observed. Hence, almost non-porous nanoparticles were obtained. Assuming that the TiFe(Nano) powder consisted of non-porous spheres, the average particle size was estimated based on the surface area to be 45.2 nm (Table 1), which is similar to the crystallite size (46.2 nm) estimated using the Scherrer equation. The scanning electron microscopy (SEM, **Figs. 2a** and **S8**) and transmission electron microscopy (TEM, **Figure S10**) images show several nanosized particles with an average size close to those estimated from the BET

surface area and XRD measurement (approximately 45 nm). The Ti/Fe molar ratios obtained by SEM-energy dispersive X-ray spectroscopy (SEM-EDS, **Figure S9**) and TEM-EDS (**Figure S11**) were similar to the stoichiometric ratio (1) of intermetallic TiFe. Calcium was not detected during the EDS analysis (**Figure S9**, **S11**), indicating the efficient washing of calcium species by post-rinsing treatments.

Table 1
BET surface area (SA) and the particle size calculated from nitrogen adsorption and XRD measurement.

| Sample | SA [$m^2/g$] | Particle size [nm] | |
|---|---|---|---|
| | | $N_2$ ads[1)] | XRD[2)] |
| $TiO_2$ (P25) | 50[3)] | 23.9 | 22.2 (anatase), 36.0 (rutile) |
| TiFe(Pre) | 39.1 | - | 21.5 (anatase), 33.4 (rutile), 21.6 ($Fe_9TiO_{15}$) |
| Fresh TiFe(Nano) | 20.0 | 45.2 | 46.2 (TiFe) |
| Used TiFe(Nano) | 12.1 | - | 43.9 (TiFe), 10.3 (Fe) |
| 1) Assumption: samples consisted of non-porous spheres with $TiO_2$ and TiFe densities of 5.01 and 6.64 $g/cm^3$, respectively. | | | |

2) Calculated using the Scherrer equation with peaks observed at 25.3°, 27.4°, 33.1°, and 43.0° for anatase, rutile, $Fe_9TiO_{15}$, and TiFe, respectively.

3) Obtained from **ref. 25**.

The surface states of fresh TiFe(Bulk) and TiFe(Nano) were investigated using X-ray photoelectron spectroscopy (XPS, **Fig. 3**). The obtained spectra were calibrated with C 1 s at 284.6 eV (**Figure S13**) and the peak identification was based on a previous report[26]. Before etching, peaks of both samples were assigned to oxidation states of Ti and Fe, suggesting that the surfaces of fresh TiFe(Bulk) and TiFe(Nano) were oxidized. After etching, peaks of metallic Ti ($Ti^0$) and Fe($Fe^0$) were observed for both samples, indicating the presence of Ti–Fe metals/alloys below the oxide layers, which is consistent with the elemental mapping results using TEM-EDS (Fig. 2b, **Figure S11 and S12**). Thus, highly crystalline intermetallic TiFe nanoparticles covered with surface oxide layers were successfully synthesized. This method is better than electrochemical methods that require higher reduction temperature[11–18]. Moreover, the particle size (45.2–46.2 nm) obtained here is much smaller than the micron sizes reported in previous works, which can be attributed to the inhibition of grain sintering by the low temperature.

**Figure S14** shows hydrogen absorption properties of TiFe(Bulk) after each activation. In the 1st and 2nd absorption cycles after the 1st activation series, similar absorption properties were obtained with the total hydrogen absorption of 0.14 wt%. After the 2nd series, this value increased to approximately 0.3 wt% and the absorption rate increased with the cycle time. After the 3rd series, absorption increased to approximately 0.67 wt% during the 5th cycle, and the rate increased with the cycle time. This indicates

that hydrogen absorption increases by repeating the activation process at high temperature and hydrogen pressure because the passive surface oxide layer breaks. This surface oxide was converted into a mixture of Fe, which facilitated the dissociation of physisorbed hydrogen molecules, and $TiO_2$ through activation, allowing hydrogen atoms to penetrate the surface and diffuse in the bulk[27]. The increase in the hydrogen absorption rate with cycling time can be attributed to the pulverization of the particles by the volume change during the hydrogen absorption and desorption cycles because of the shortening of the hydrogen diffusion path in the bulk and the increase in the surface area[27].

Figure 4 shows a comparison between the hydrogen absorption properties of TiFe(Nano) and TiFe(Bulk) after the 5th absorption cycle conducted after each activation series. In TiFe(Bulk), the absorption increased with repeating the activation process, while that in TiFe(Nano) was only 0.06 wt% in the 5th cycle after the 1st activation series. Similar properties were obtained during the 1st to 5th cycles. Those after the 5th cycle of the 2nd and 3rd activation series were similar to that obtained after the 1st one, indicating that the activation and hydrogen sorption-cycling process did not improve the hydrogen absorption properties of TiFe(Nano).

The non-activated TiFe(Nano) was compared to TiFe(Bulk) powders by characterization using XRD (**Figure S15**) and SEM (Figs. 5a, b and **Figure S16**). $N_2$ adsorption (**Figure S17**) and TEM-EDS (**Figures S18, S19**) were also conducted. XRD measurements showed that the used TiFe(Nano) partially decomposed to form $TiFe_{39}$ or/and Fe, but a TiFe phase remained. However, no extra phases were observed in the used TiFe(Bulk). Clear cracks were observed in the used TiFe(Bulk) (Fig. 5a, **Figure S16a**), which is often observed in activated TiFe alloys[4], while no cracks were observed in the used TiFe(Nano) (Fig. 5b, **Figure S16b**). The morphology and particle size of the used TiFe(Nano) were similar to those of the fresh TiFe(Nano) because they were maintained through the surface oxide layers. This can be attributed to the followings: First, the breakdown of the passive oxide layer was not facilitated because its large surface oxygen ratio due to the high surface area compared to TiFe(Bulk). Second, no particle pulverization by volume change occurred during hydrogen sorption because the hardness of TiFe(Nano) is six times larger than that of TiFe(Bulk) due to the Hall-Petch contribution[28,29] (**Table S1**). Thus, it was too difficult to fracture TiFe(Nano) that was composed of non-porous spheres. Therefore, the oxidized surface nanoparticles of alloys, such as TiFe, that exhibit surface activation difficulty, hardly absorb hydrogen by conventional activation treatments. To improve the hydrogen absorption properties of TiFe(Nano), future studies may investigate adding a third element to TiFe(Nano) nanoparticles to increase the catalytic active surface, promoting hydrogen diffusion, and decrease the fracture toughness of the alloy[4].

# Conclusions

Intermetallic TiFe nanoparticles were chemically prepared at 600 °C in a molten LiCl–$CaH_2$ mixture. The prepared nanopowder exhibited the highly crystalline structure of intermetallic TiFe and a high BET surface area of 20.0 $m^2/g$. The BET, XRD, and SEM results confirmed the formation of nanosized

particles of 45.2–46.2 nm. Compared to previous electrochemical methods, the proposed method allowed a lower temperature reduction, resulting in smaller nanoparticles. This was achieved using $CaH_2$ as a superior reducing agent in molten LiCl. It was also demonstrated that TiFe nanoparticles were difficult to activate compared to the bulk powder, since the oxidized surface layers of the nanoparticles were stabilized, which prevents the morphological change necessary for the activation.

# Declarations


### Acknowledgements

We acknowledge the Advanced Characterization Nanotechnology Platform of the University of Tokyo and the Center for Instrumental Analysis Ibaraki University for sample characterization. The authors thank Prof. Noda at Waseda University for his support in SEM-EDS measurement.


### Author contributions statement

Y.K. designed the study, performed the experiments for TiFe synthesis. S.Y., S.Y. and N.H. conducted the hydrogen absorption experiments. S.T. and R.K. analysed the prepared nanoparticles and verified the results. All authors reviewed the manuscript.

### Competing interests

The authors declare no competing interests.

# References


1. G. Sandrock, J. Alloys Comp., 1999, 293–295, 877.
2. N. A. A. Rusman and M. Dahari, Int. J. Hydrogen Energy, 2016, 41, 12108.
3. J. J. Reilly and R. H. Wiswall Jr., Inorg. Chem., 1974, 13, 218.
4. G. K. Sujan, Z. Pan, H. Li, D. Liang and N. Alam, Crit. Rev. Solid State, DOI: 10.1080/10408436.2019.1652143.
5. M. Bououdina, D. Grant and G. Walker, Int. J. Hydrogen Energy, 2006, 31, 177.
6. V. Bérubé, G. Radtke, M. Dresselhaus and G. Chen, Int. J. Energy Res, 2007, 31, 637.
7. N. Z. Abd. K. Khafidz, Z. Yaakob, K. L. Lim and S. N. Timmiati, Int. J. Hydrogen Energy, 2016, 41, 13131.
8. A. Schneemann, J. L. White, S. Y. Kang, S. Jeong, L. F. Wan, E. S. Cho, T. W. Heo, D. Prendergast, J. J. Urban, B. C. Wood, M. D. Allendorf and V. Stavila, Chem. Rev., 2018, 118, 10775.
9. R. A. Varin and T. Czujko, Mater. Manuf. Process, 2002, 17, 129.
10. V. Yu. Zadorozhnyy, G. S. Milovzorov, S. N. Klyamkin, M. Yu. Zadorozhnyy, D. V. Strugova, M. V. Gorshenkov and S. D. Kaloshkin, Pro. Nat. Sci. Mater., 2017, 27, 149.

11. M. Ma, D. Wang, X. Hu, X. Jin and G. Z. Chen, Chem. Eur. J., 2006, 12, 5075.
12. S. Tan, T. Örs, M. K. Aydınol, T. Öztürk and I. Karakaya, J. Alloys Comp., 2009, 475, 368.
13. T. Tsuchiya, N. Yasuda, S. Sasaki, N. Okinaka and T. Akiyama, Int. J. Hydrogen Energy, 2013, 38, 6681.
14. M. Deguchi, N. Yasuda, C. Zhu, N. Okinaka and T. Akiyama, J. Alloys Comp., 2015, 622, 102.
15. L. Xiong, Y. Hua, C. Xu, J. Li, Y. Li, Q. Zhang, Z. Zhou, Y. Zhang and J. Ru, J. Alloys Comp., 676 (2016) 383–389.
16. Z. Zhou, Y. Hua, C. Xu, J. Li, Y. Li, L. Xiong and Z. Zhang, J. Alloys Comp., 726 (2017) 1124–1131.
17. Z. Zhou, Y. Hua, C. Xu, J. Li, Y. Li, Q. Zhang, Y. Zhang and W. Kuang, Ionics, 2017, 23, 213.
18. Z. Zhou, Y. Zhang, Y. Hua, P. Dong, C. Xu, Y. Li and D. Wang, Electrochimica Acta, 2018, 271, 490.
19. Y. Kobayashi, Synthesis of Porous Ni3Al Intermetallic Nano-compounds in a Molten LiCl with an Assistance of CaH2 as a Structure-Controlling Agent, Chem. Lett., 2019, 48(12), 1496–1499.
20. Y. Kobayashi, S. Tada and R. Kikuchi, Mesoporous Intermetallic NiAl Nanocompound Prepared in a Molten LiCl Using Calcium Species as Templates, Chem. Lett., 2020, 49(4), 341–343.
21. Y. Kobayashi, S. Tada and R. Kikuchi, Simple Chemical Synthesis of Ternary Intermetallic RENi2Si2 (RE = Y, La) Nanoparticles in Molten LiCl–CaH2 System, Mater. Trans., 2020, 61(5), 1037–1040.
22. Y. Kobayashi, S. Tada and R. Kikuchi, Effects of Porosity and Ni/Al Molar Ratio in Ni-Al Oxide Precursors on Porous Intermetallic Nickel Aluminide Nanopowders Prepared by Chemical Route, J. Chem. Eng. Jpn., 2020, 53(9), 562–568.
23. Y. Kobayashi, S. Tada and R. Kikuchi, Simple Chemical Synthesis of Intermetallic Pt2Y Bulk Nanopowder, Mater. Adv., 2020, 1(7), 2202–2205.
24. Y. Kobayashi, M. Sohmiya, S. Tada and R. Kikuchi, Low-Temperature Synthesis of Single Phase Intermetallic NiZn bulk Nanopowder in a Molten LiCl-KCl with a CaH2 as a reducing agent, J. Jpn. Petrol. Inst., 2020, 63(6), 380–387.
25. Y. Kobayashi, R. Kanasaki, T. Nozaki, R. Shoji and K. Sato, J. W. E. T., 2017, 15, 35.
26. K. Edalati, J. Matsuda, M. Arita, T. Daio, E. Akiba and Z. Horita, Appl. Phys. Lett., 2013, 103, 143902.
27. L. Schlapbach, and T. Riesterer, Appl. Phys. A, 1983, 32, 169.
28. E. O. Hall, Proc. Phys. Soc.B 1951, 64 (9), 747.
29. N. J. Petch, J. Iron Steel Inst. 1953, 174, 25.

# Figures

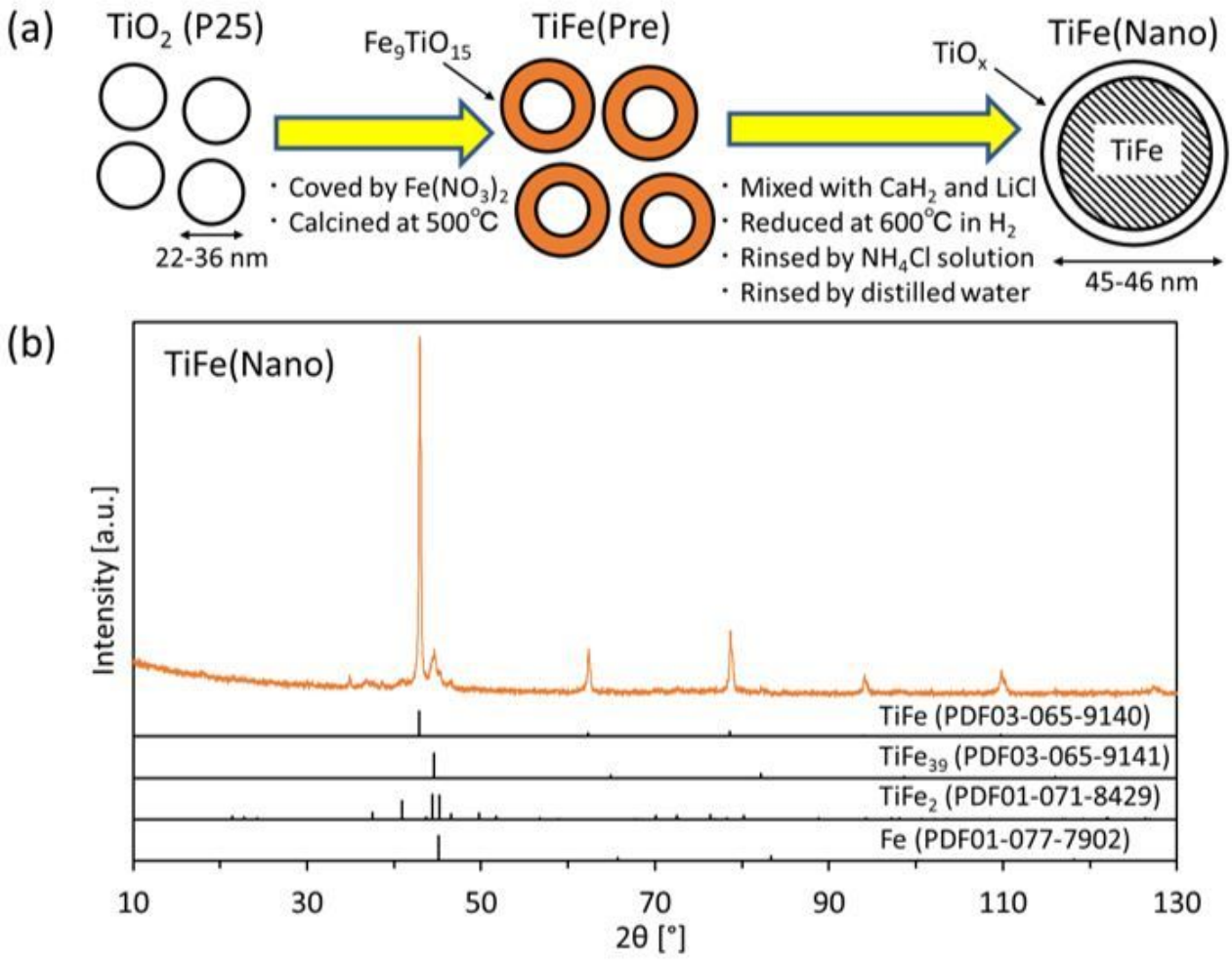


**Figure 1**

(a) TiFe nanoparticle synthesis and (b) XRD patterns of TiFe(Nano).

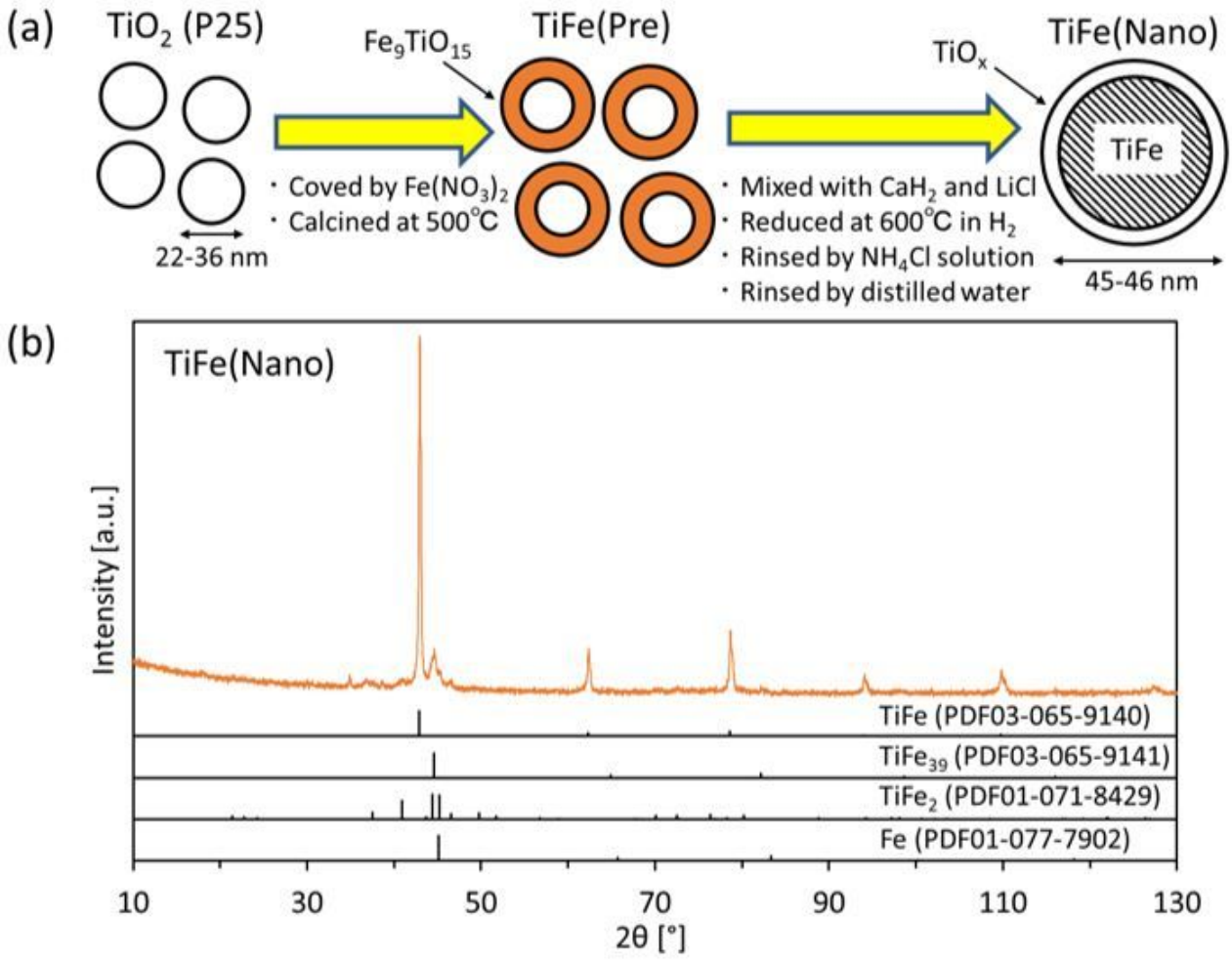


**Figure 1**

(a) TiFe nanoparticle synthesis and (b) XRD patterns of TiFe(Nano).

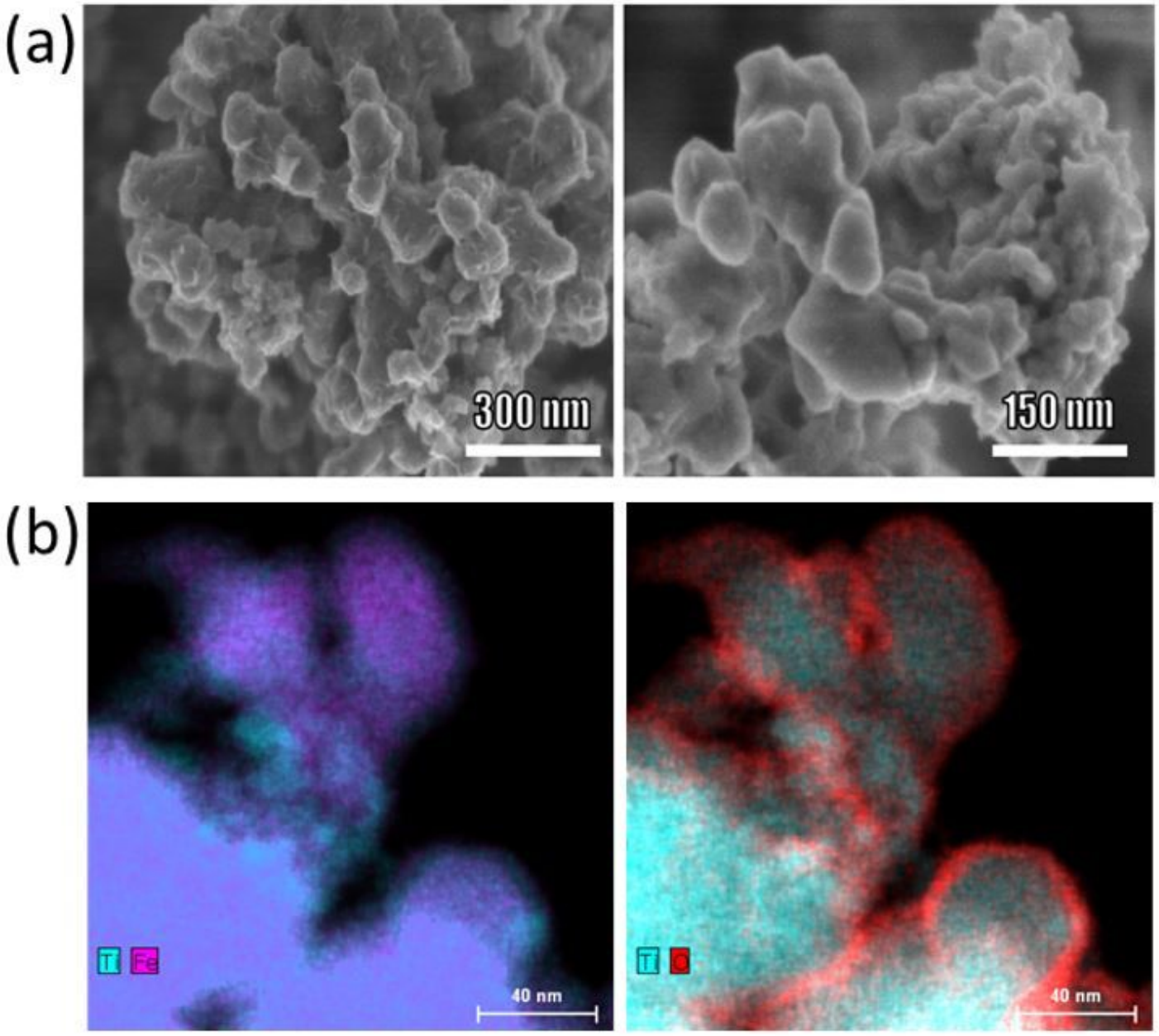


## Figure 2

(a) SEM images of fresh TiFe(Nano) and (b) elemental mapping by TEM-EDS (Ti: blue, Fe: purple, O: red).

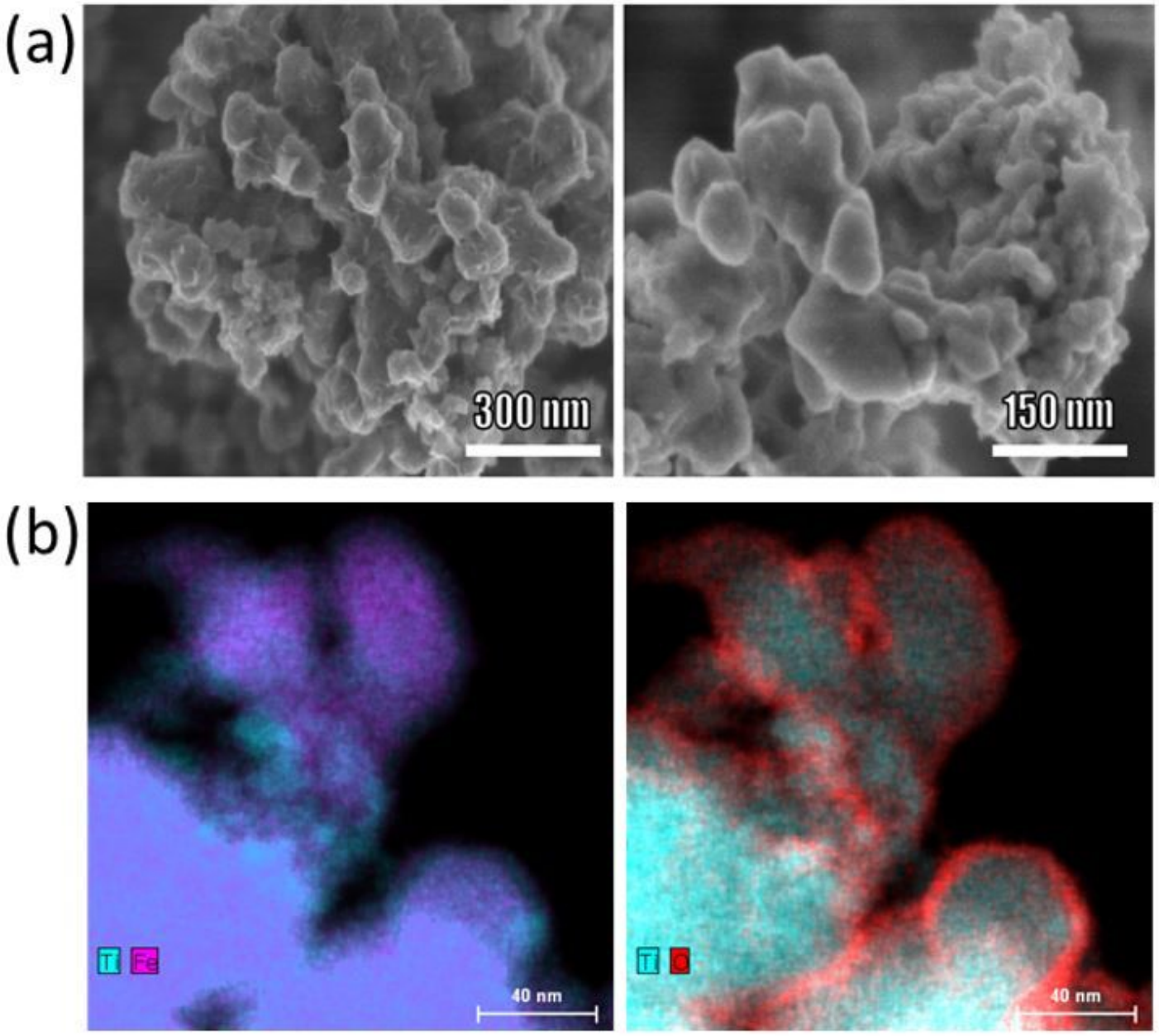


## Figure 2

(a) SEM images of fresh TiFe(Nano) and (b) elemental mapping by TEM-EDS (Ti: blue, Fe: purple, O: red).

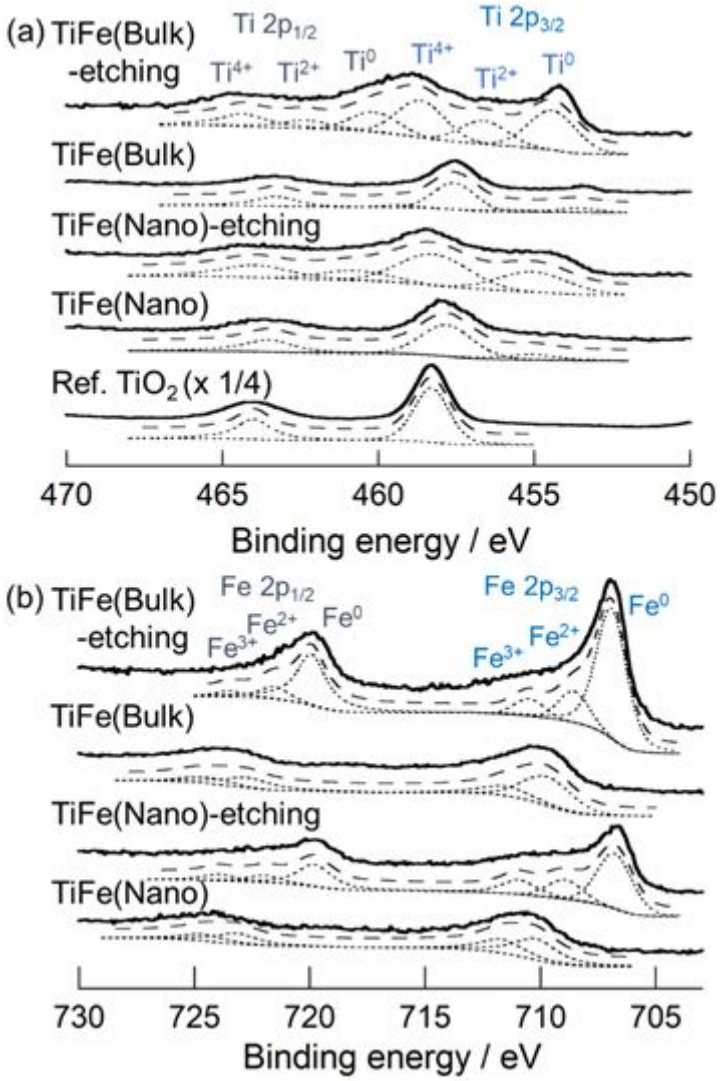


## Figure 3

XPS spectra of (a) Ti 2p and (b) Fe 2p for fresh TiFe(Nano) and TiFe(Bulk).

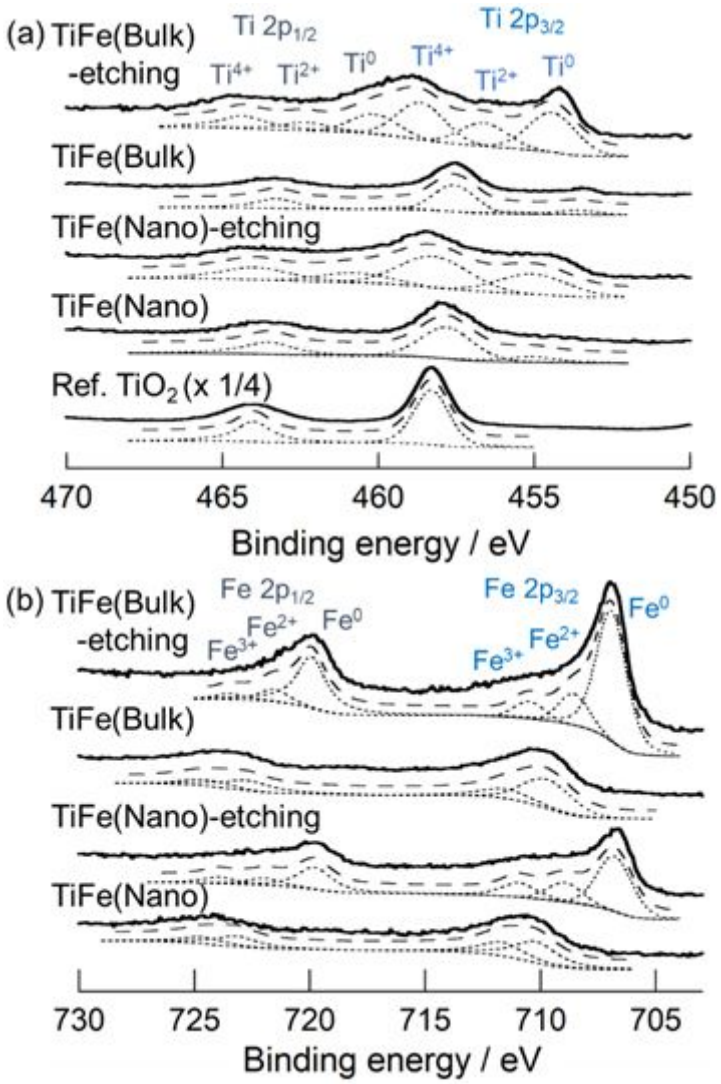


## Figure 3

XPS spectra of (a) Ti 2p and (b) Fe 2p for fresh TiFe(Nano) and TiFe(Bulk).

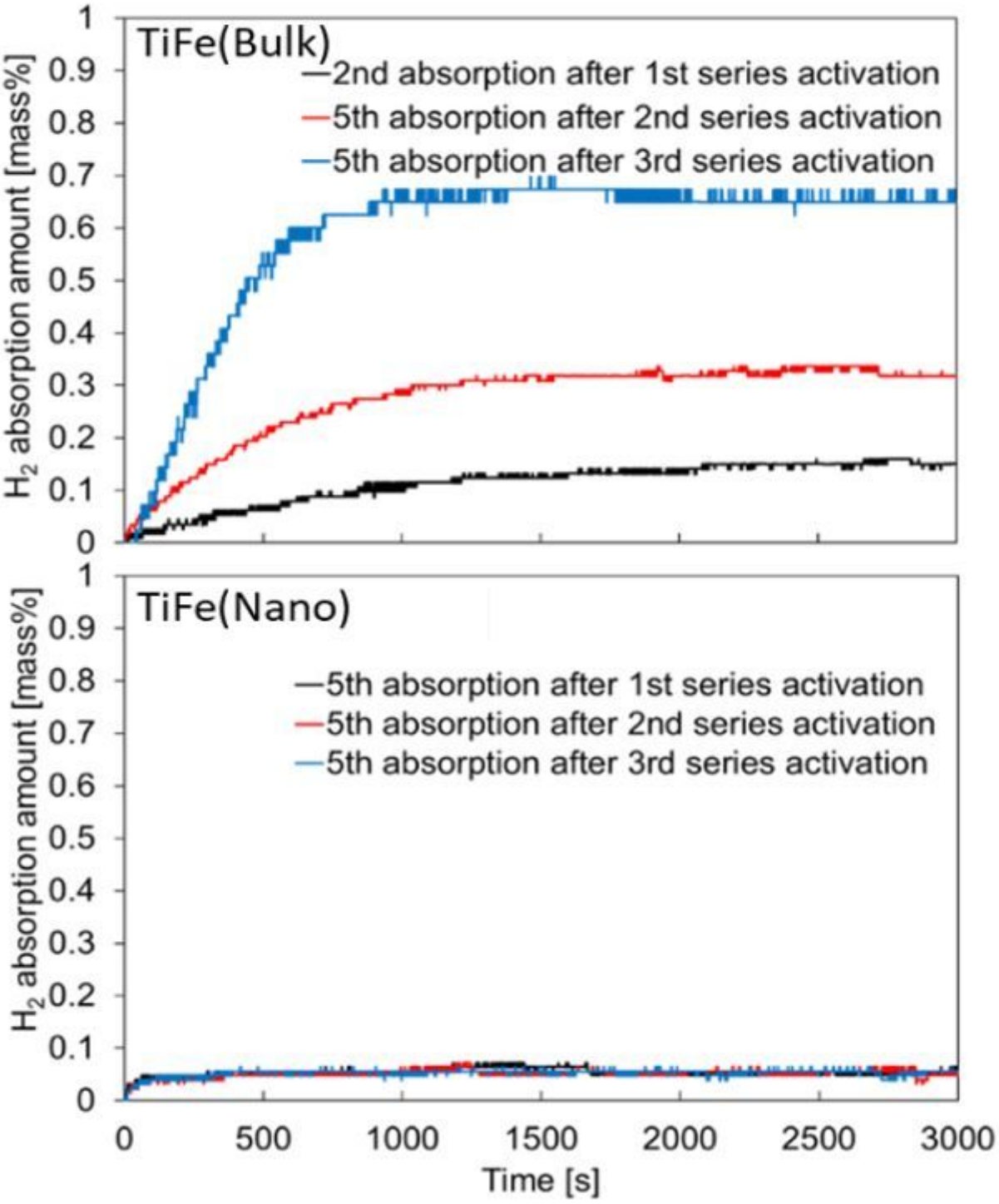


**Figure 4**

Hydrogen absorption properties of TiFe(Bulk) and TiFe(Nano) after the 2nd and 5th absorption cycles after activation.

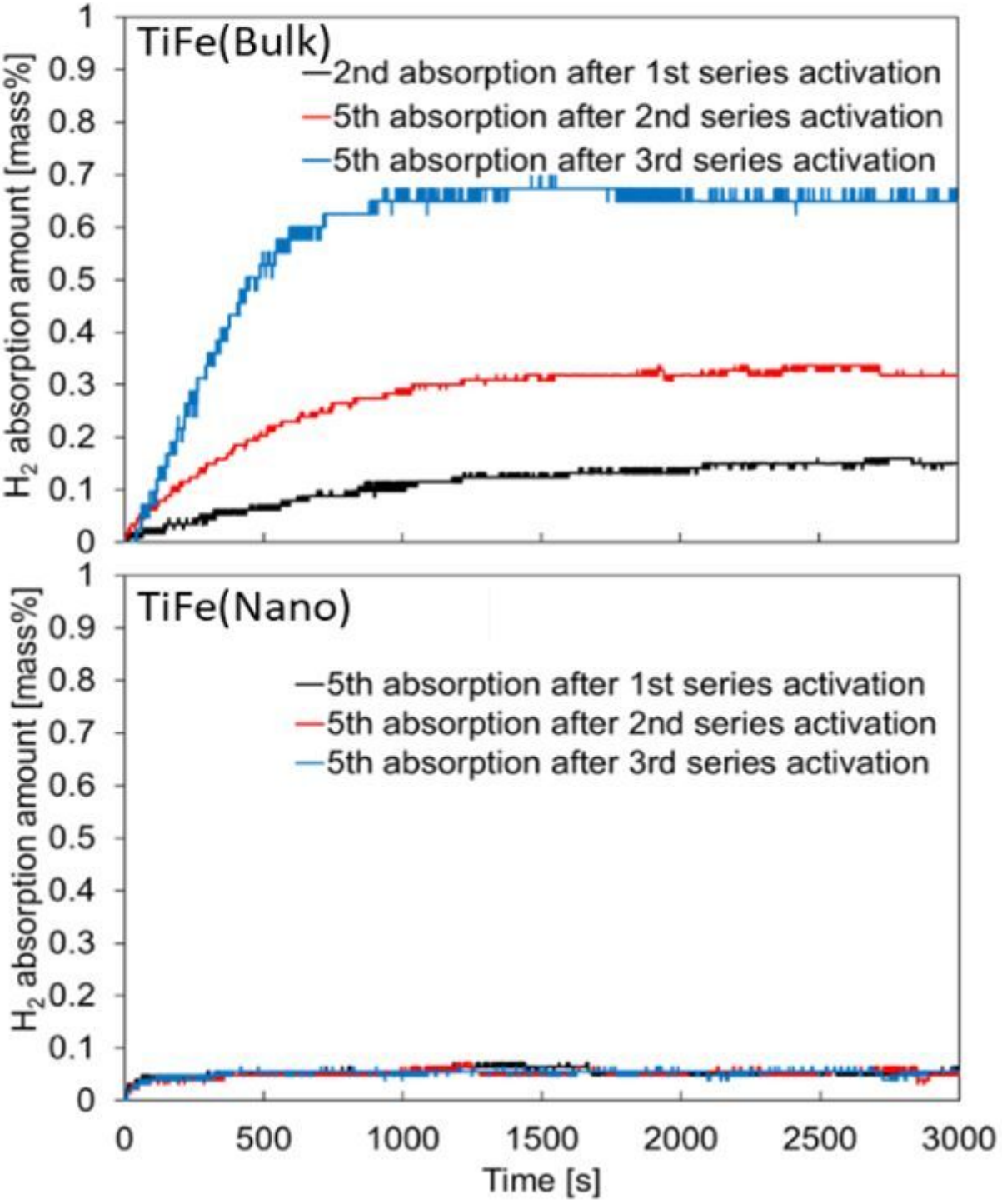


**Figure 4**

Hydrogen absorption properties of TiFe(Bulk) and TiFe(Nano) after the 2nd and 5th absorption cycles after activation.

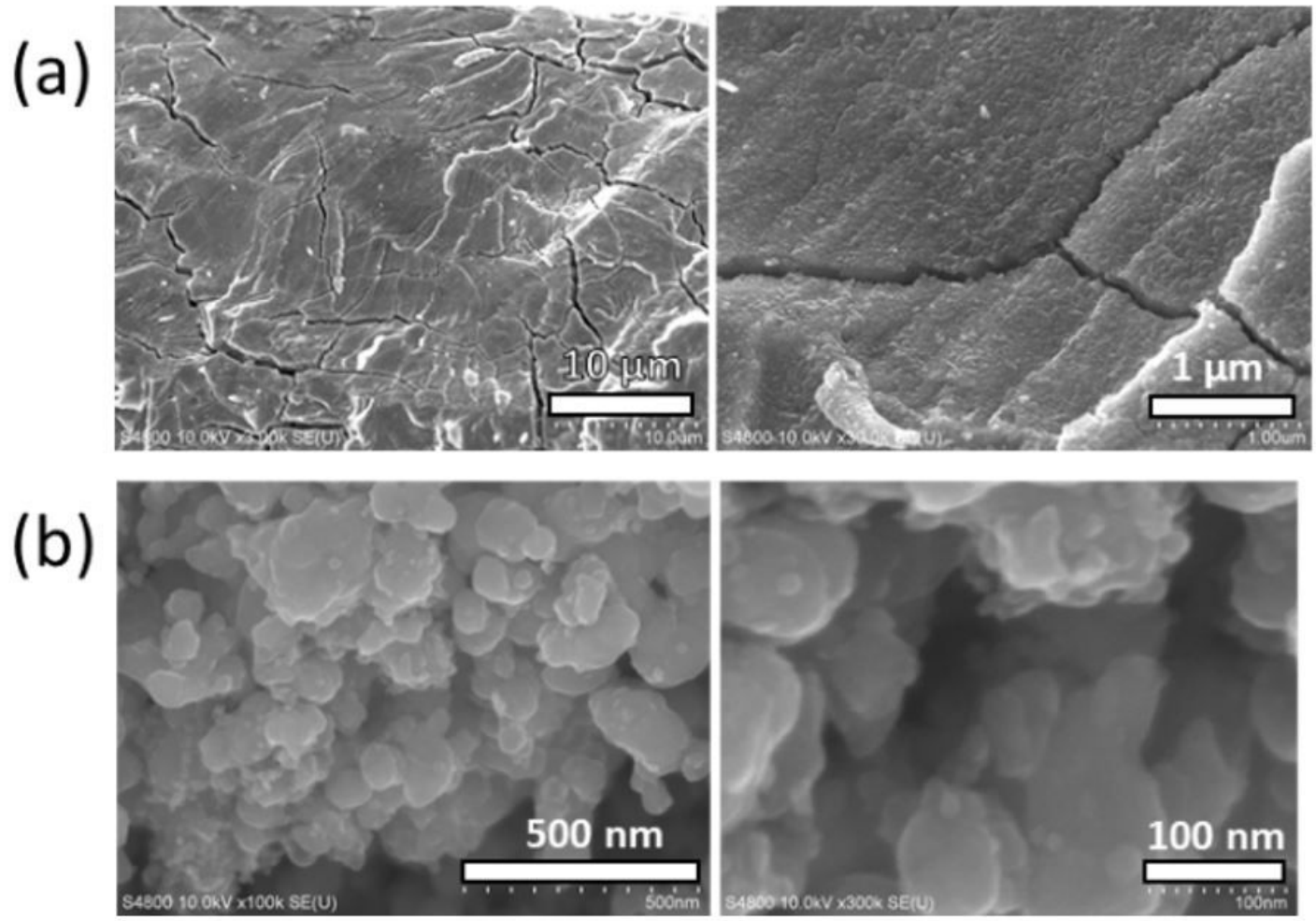


**Figure 5**

SEM images of (a) used TiFe(Bulk) and (b) used TiFe(Nano).

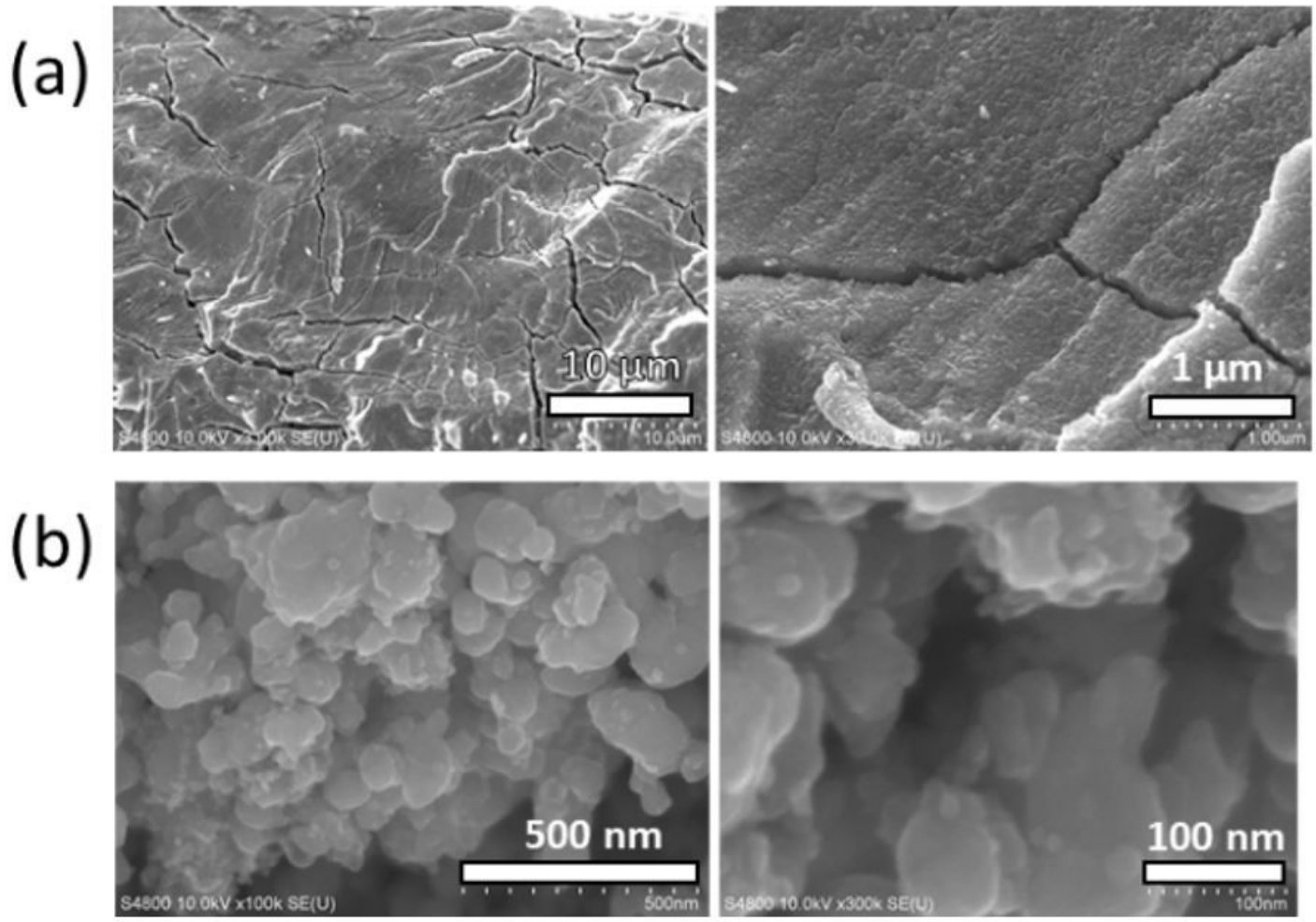


**Figure 5**

SEM images of (a) used TiFe(Bulk) and (b) used TiFe(Nano).

## Supplementary Files

This is a list of supplementary files associated with this preprint. Click to download.

- 11262020SuppInfSciRep.docx
- 11262020SuppInfSciRep.docx